J. Phys.: Condens. Matter **12** (2000) 4947–4958. Printed in the UK PII: S0953-8984(00)12985-6

# The effect of Coulomb correlation and magnetic ordering on the electronic structure of two hexagonal phases of ferroelectromagnetic $YMnO_3$

J E Medvedeva†, V I Anisimov†, M A Korotin†, O N Mryasov‡ and A J Freeman‡

† Institute of Metal Physics, Yekaterinburg, Russia

‡ Department of Physics and Astronomy, Northwestern University, Evanston, IL 60208-3112, USA

Received 31 March 2000

**Abstract.** The electronic structure of $YMnO_3$ in its high- and low-temperature hexagonal phases has been investigated within the local spin-density approximation (LSDA) and by the LSDA + $U$ method which takes into account the local Coulomb interaction between d electrons of transition-metal ions. In contrast to the case for orthorhombic manganites, the $d^4$-configuration degeneracy is already lifted in the high-temperature symmetric hexagonal phase, indicating that $Mn^{3+}$ is not a Jahn–Teller ion; hence, we argue that the lowering of the symmetry is not connected with Jahn–Teller instability in hexagonal $YMnO_3$. Each of these two hexagonal phases is found to be semiconducting, with a band gap of about 1.5 eV. It is shown that magnetism and correlation effects are important in band-gap formation for both crystal structures. Using the Green function method, we estimated the Néel temperature from the calculated effective exchange interaction parameters, and found it to be in good agreement with experiment.

## 1. Introduction

The hexagonal yttrium and rare-earth manganites with the overall formula $RMnO_3$ (R = Y, Ho, Er, Tm, Yb, Lu) [1, 2] are ferroelectromagnetic compounds possessing both magnetic and ferroelectric ordering. It is known [3] that these compounds have antiferromagnetic properties with $T_N < 80$ K. The ferroelectric transition in these manganites occurs at a high Curie temperature (600–990 K) [3, 4], where the polar space group $P6_3cm$ is replaced by the centrosymmetric group $P6_3/mcm$. Another phase transition resulting in the crystal structure with a smaller hexagonal lattice cell ($P6_3/mmc$) was found at 1273 K [5]. In spite of the large difference between the ferroelectric and magnetic ordering temperatures, the observation of anomalies in the dielectric constant and loss tangent in $YMnO_3$ are indicative of coupling between the ferroelectric and magnetic order [6]. As distinct from that for other ferroelectromagnetics of the $ABO_3$ type with orthorhombic crystal structure, the mechanism of the electric and magnetic phase transitions in hexagonal manganites has not been the subject of numerous experimental and theoretical studies.

The hexagonal phase of $RMnO_3$ (R = Y, Ho, Er) may be transformed at high temperature (1270 K) and pressure (35–40 kbar) to the orthorhombic perovskite-type phase [7], which is typical for rare-earth manganites with R = La, Ce, Pr, Nd, Sm, Eu, Gd, Tb, Dy. The existence of the hexagonal $RMnO_3$ structure, as compared with the orthorhombic perovskite-type one, is

0953-8984/00/234947+12$30.00  

usually explained by the smaller values of the rare-earth-ion radii and the presence of covalent Mn–O bonds due to $3d^4sp^3$ hybridization [8].

Among rare-earth manganites, the doped $LaMnO_3$ compounds are the most extensively investigated due to the striking correlation between spin, electronic and lattice subsystems that results in colossal-magnetoresistance phenomena. It is now accepted that the insulating ground state of $LaMnO_3$ is driven by lattice distortions and AFM ordering [9, 10]. $LaMnO_3$ consists formally of a $Mn^{3+}$ $d^4$ ion in an octahedral crystal field where for the high-spin configuration the $t_{2g}$ energy levels are filled and one electron occupies the doubly degenerate $e_g$ spin-up level. As commonly accepted, such an electronic configuration results in a Jahn–Teller (JT) instability. As for $LaMnO_3$, strong JT lattice distortions were also observed [7] for the orthorhombic phase of $YMnO_3$. One may assume a similar situation for hexagonal $YMnO_3$ which also has $Mn^{3+}$ ($d^4$) ions. Indeed, small magnetoelectric and magnetoresistive effects were also detected in hexagonal $YMnO_3$ from observations of anomalies in the dielectric constant and loss tangent [6].

Thus, our work is concerned with hexagonal $YMnO_3$, which is, in addition, of interest because of its device applications: $YMnO_3$ was proposed recently as a new candidate for use in non-volatile memory devices [11]. The analogy with the currently used $La_{1-x}Sr_xMnO_3$ system allowed several authors [12] to consider strontium-doped $YMnO_3$ as a potential cathode material for solid oxide fuel cells.

An important problem arising in the study of the electronic properties of manganites is the applicability of traditional LSDA methods for strongly correlated systems. It was shown that the Coulomb interaction inside the Mn d shell can play a significant role in the orbital ordering of undoped La(Ca)$MnO_3$ [13] and undoped or Ca-doped orthorhombic $PrMnO_3$ [14]. The LSDA + $U$ approach provides a more reliable description of the electronic structure of correlated materials with charge, spin and orbital ordering than does the LSDA scheme [15].

The present investigation is the first attempt to establish the electronic structure of low- and high-temperature hexagonal $YMnO_3$ phases using the LSDA and LSDA + $U$ [15] approximations. The interplay and relative importance of different factors: (i) structural changes, (ii) magnetic ordering and (iii) correlation effects in the electronic structure formation are considered in detail for two hexagonal $YMnO_3$ phases. We show that although proper magnetic ordering leads to insulating ground states for both crystal structures, the Coulomb interaction correction to the one-electron LDA plays an important role in reproducing band gaps. We demonstrate that the structural changes associated with the transition from the high-symmetry to the low-symmetry phase of hexagonal $YMnO_3$ almost do not affect its electronic and orbital structures. In striking contrast to the case for the perovskite manganites, the lowering of the symmetry is not connected with a Jahn–Teller instability. We estimate the Néel temperature by calculating effective exchange interaction parameters; this estimate may be additional evidence for the reliability of our calculations.

## 2. Crystal structure and computational approach

As stated above, the crystal structure of $YMnO_3$ above 1273 K has the hexagonal space group $P6_3/mmc$ with two formula units and $a = 3.61$ Å and $c = 11.39$ Å [5]. This higher-symmetry structure may be considered as the prototype of the $YMnO_3$ structure at room temperature. The primitive cell of the high-temperature phase contains two hexagonal layers with equivalent Mn sites that are fivefold coordinated by oxygens (figure 1(a)). The Mn–O distances with the planar O(1) oxygens (2.09 Å) are substantially larger than with the apical O(2) oxygens (1.88 Å).

The more distorted hexagonal structure ($P6_3cm$) with six formula units per unit cell (30 atoms/cell) was observed below the ferroelectric transition temperature (figure 1(b)). The

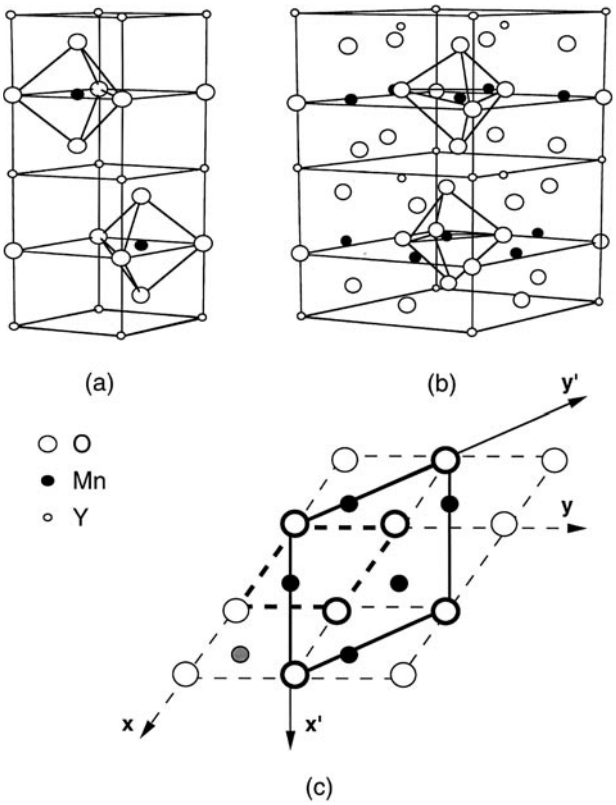


**Figure 1.** The hexagonal crystal structure of $YMnO_3$: (a) the high-temperature paraelectric $P6_3/mmc$ phase; (b) the ferroelectric $P6_3cm$ phase; (c) the connection between crystal axes: $x$, $y$ for the $P6_3/mmc$ phase (dashed line) and $x'$, $y'$ for the $P6_3cm$ phase (solid line). Thick lines indicate the projection of the corresponding unit cell in the $a$–$b$ plane.

lattice parameters are equal to $a = 6.125$ Å and $c = 11.41$ Å [2]. The atomic positions, known only for $LuMnO_3$, were taken from reference [2]. The equivalent Mn ions are in 6(c) positions forming a simple hexagonal net. The important aspects of this structure are the tilting of the $MnO_5$ bipyramids with respect to the $c$-axis and its stronger distortion (cf. figure 1(a) and figure 1(b)). Instead of one type of apical oxygen for the high-temperature phase, there are two non-equivalent atoms O(1) and O(2) with Mn–O distances equal to 1.96 Å and 1.84 Å, respectively. In the plane, we have two pseudo-planar O(3) and O(4) atoms, with Mn–O distances equal to 1.96 Å and 2.08 Å.

The connection between these two phases is shown in figure 1(c). The $a$-parameter differs by a factor of $\sqrt{3}$. Since the $c$-parameter is approximately the same in the two phases, the number of formula units increases by a factor of three for the low-temperature phase (the tripling of the unit cell in the plane).

In the Mott–Hubbard insulators, where the orbital dependence of the one-electron potential is essential for the description of the splitting of the electron spectrum between the lower occupied and the higher unoccupied Hubbard bands, the LSDA gives qualitatively incorrect results. The main feature of the LSDA + $U$ method is that the usual LDA single-particle potential is augmented with orbital and spin dependencies, as one would find in a mean-field calculation for a Hubbard model containing on-site $U$-interactions (on-site Coulomb

interactions) and $J$-interactions (Hund's rule exchange interactions). The LSDA + $U$ calculations were carried out in the framework of the linear muffin-tin orbital method in the atomic sphere approximation (LMTO-ASA) [16] using the Stuttgart TBLMTO-47 code. The same code was used in standard LSDA calculations. The exchange–correlation potential used is the von Barth–Hedin–Janak form [17]. The values of $U = 8$ eV and $J = 0.88$ eV used were obtained from the constrained LSDA supercell calculations.

## 3. Electronic structure of the high-temperature phase

Electronic structure calculations for the high-temperature phase were performed for 14 atoms/unit cell, including four empty spheres, which were introduced because this structure is not sufficiently closely packed. For the non-spin-polarized case, the Fermi level falls in the region of a large peak in the density of states, suggesting a Stoner instability of the non-magnetic (NM) state. Indeed, the ferromagnetic (FM) state is calculated to have a lower energy (by 7.85 eV) than the non-magnetic state. A small direct gap ($\sim$0.01 eV) was obtained for the FM state in the LSDA calculation. This small gap can be taken as an indication of a pseudo-Jahn–Teller effect, arising in the case where the d levels have an energy separation $\Delta E \sim kT$.

The FM ordering is not natural for this compound, where triangular lattice antiferromagnetism in the basal $xy$-plane is expected from experiment [18] and theoretical considerations [19]. We then simulated the complicated non-collinear AFM state of hexagonal $YMnO_3$ by a collinear AFM state in an extended supercell with three Mn atoms in the basal plane, two of them with a spin-up magnetic moment and one with a spin-down moment. We found that this AFM state is more favourable than the FM state by 6.10 eV. Figure 2 shows the density-of-states results obtained for such an AFM ordering within the LSDA. The antiferromagnetic spin alignment leads to an effective decrease of the Mn 3d and O 2p hybridization and results in narrower bands. The states near the top of the valence band have predominantly Mn 3d($x^2 - y^2$)–O(1) 2p($x$, $y$) character while the lowest unoccupied subband has Mn 3d($3z^2 - r^2$)–O(2) 2p($z$) character (which is highest in energy and is the only unoccupied majority-spin d orbital since the shortest Mn–O bond is with the apical oxygen). The increase of $E_g$ from its nearly zero value for the FM case to 0.47 eV for the AFM case indicates the importance of taking into account the correct magnetic ordering.

The $D_{3h}$ crystal-field symmetry of bipyramidal oxygen ions around the Mn ion splits the Mn d levels into three components ($a_1$ and two doubly degenerate e states [20]) in contrast with the two components ($e_g$ and $t_{2g}$) in $LaMnO_3$ having its octahedral oxygen coordination. For this crystal structure, the pairs of Mn orbitals (d($xz$), d($yz$)) and ((d($x^2-y^2$), d($xy$)) are transformed according to the same doubly degenerate point group e representation. We demonstrate results only for one orbital of each spatial type (d($xz$) $\equiv$ d($yz$) and d($x^2 - y^2$) $\equiv$ d($xy$)) in figure 2.

In the high-temperature symmetric phase, the crystal-field splitting between d orbitals of $a_1$ and e symmetry is already large (d-band centres of the occupied and empty bands are separated by $\sim$2.0 eV). Thus, the distortions existing in the high-temperature structure have already removed the d-state degeneracy and so the Jahn–Teller instability normally associated with a $d^4$ configuration is unlikely in hexagonal $YMnO_3$. Hence, we argue that this is one of the striking differences between orthorhombic and hexagonal $YMnO_3$.

The top of the valence band is formed by Mn 3d states of ($xy$, $x^2 - y^2$) symmetry. The corresponding band is rather broad and looks similar to the partially filled band formed by $e_g$ orbitals in orthorhombic $LaMnO_3$. If this band were also partially filled, one could expect strong Jahn–Teller distortions and the orbital ordering analogous to that observed in

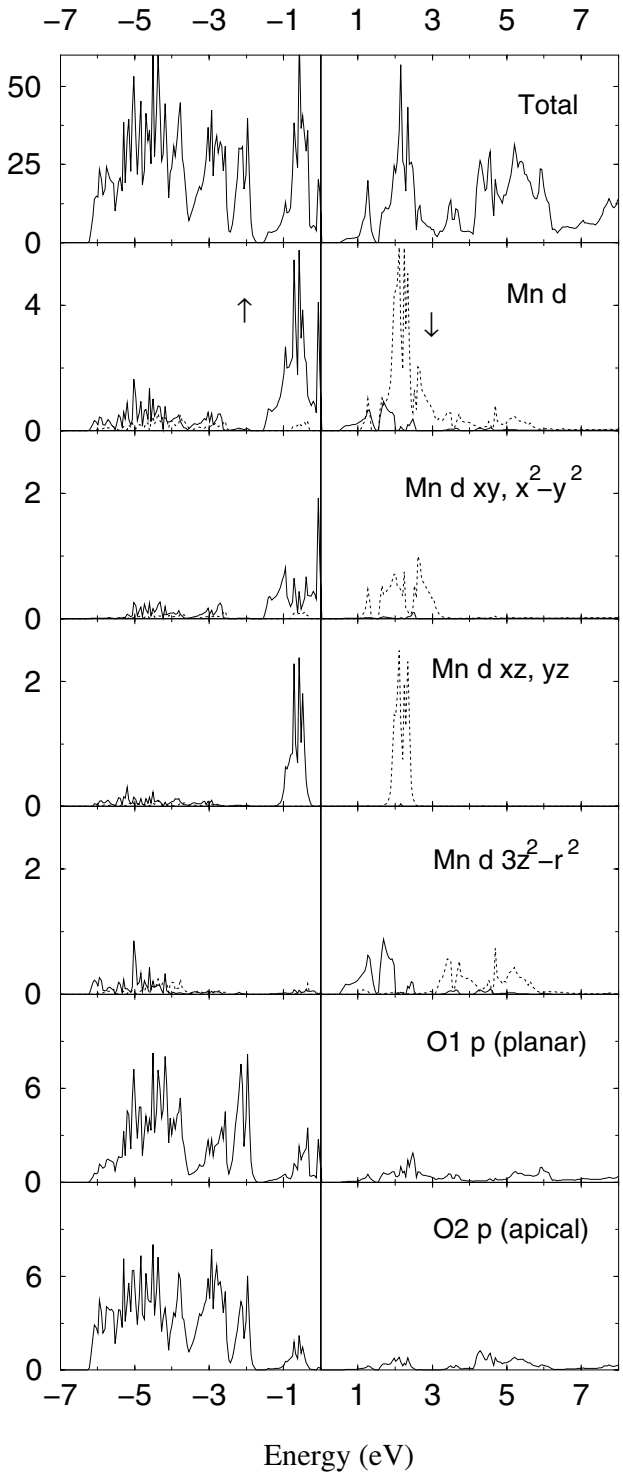


**Figure 2.** The total and partial densities of states (DOS) from the LSDA calculation of the high-temperature AFM phase. Solid lines are for majority spin and dashed lines for minority spin.

the orthorhombic manganites. We propose that hexagonal $YMnO_3$ be doped with divalent ions (with small ionic radii to preserve the hexagonal crystal structure) in order to test our prediction.

The effect of electron correlation was investigated for both the FM and AFM states within the LSDA + $U$ method. Values of $U = 8$ eV and $J = 0.88$ eV, obtained from constrained LSDA supercell calculations, as described in [21, 22], are similar to the $U = 10$ eV and $J = 0.9$ eV values for both $LaMnO_3$ and $CaMnO_3$ calculated in [13] and the $U = 7.9$ eV and $J = 0.9$ eV values for the Pr–Ca–Mn–O system obtained in [14].

The electronic structure for the FM and AFM cases obtained in our LSDA + $U$ calculations is semiconducting with band gaps of 0.19 eV and 1.28 eV, respectively. Hence, the incorporation of the local Coulomb interaction between d electrons of the Mn ions in the framework of the LSDA + $U$ approximation leads to an increase of the band gap. Thus, both magnetic ordering and correlation effects play an important role in band-gap formation.

Let us now compare the electronic spectra obtained in the LSDA and LSDA + $U$ approximations (cf. figures 2 and 3). Because of the large $U$-value, the occupied and unoccupied parts of the d bands calculated in LSDA + $U$ are split by ∼8 eV. As a result, the centres of the occupied d states are shifted to the low-energy region and give a smaller contribution near $E_F$. By contrast the weight of the oxygen 2p states increases at the top of the valence band. This means that the LSDA + $U$ approach results in decreasing the p–d hybridization near $E_F$. The calculated Mn magnetic moments, 3.56 $\mu_B$ (LSDA) and 3.99 $\mu_B$ (LSDA + $U$) for the AFM case, also demonstrate the weaker Mn 3d–O 2p hybridization in the LSDA + $U$ electronic structure of $YMnO_3$.

## 4. Electronic structure of the low-temperature phase

For the low-temperature structure, the calculations were performed for a unit cell with 42 atoms including 12 empty spheres. We found that for this phase, the non-magnetic (NM) state is also characterized by a large value of the density of states (DOS) at the Fermi level. The DOS obtained for the FM state (which is 9.55 eV lower in energy than the NM state) in the LSDA is similar to the DOS of the high-temperature phase in the same magnetic configuration—a very small energy band gap ($E_g \sim 0.01$ eV) and a magnetic moment of 3.72 $\mu_B$. For the collinear AFM ordering, see figure 4, which is used to simulate the experimental non-collinear ground state in the same way as for the high-temperature phase, the LSDA scheme predicts an indirect band gap, $E_g = 0.11$ eV. The experimental optical gap is about 1.27 eV [23], which is one order of magnitude greater than our LSDA result. This discrepancy can be taken as a manifestation of the typical underestimation of the band gap in LSDA, but aggravated in this case by the strong correlation.

For the FM and AFM cases, the LSDA + $U$ calculations lead to substantially increased $E_g$-values of 0.79 eV and 1.36 eV, respectively. Thus, the value of $E_g$ obtained in the LSDA + $U$ scheme for the AFM case is in much better agreement with experiment than are the LSDA results. Our calculations demonstrate that the structural changes associated with the transition from the high-symmetry to the low-symmetry phase almost do not affect the band gap. This emphasizes the importance of magnetic ordering and correlation for understanding the electronic structure and properties.

It should be noted that the low-temperature structure is characterized by stronger 3d–2p hybridization, which appears in the slightly wider bands (figure 5) and results in a decrease of the Mn magnetic moments. For the low-temperature AFM phase, we obtained 3.50 $\mu_B$ (LSDA) and 3.92 $\mu_B$ (LSDA + $U$). We suppose that the oxygen displacement towards Mn due to p–d hybridization is the driving mechanism for the phase transition in $YMnO_3$. This

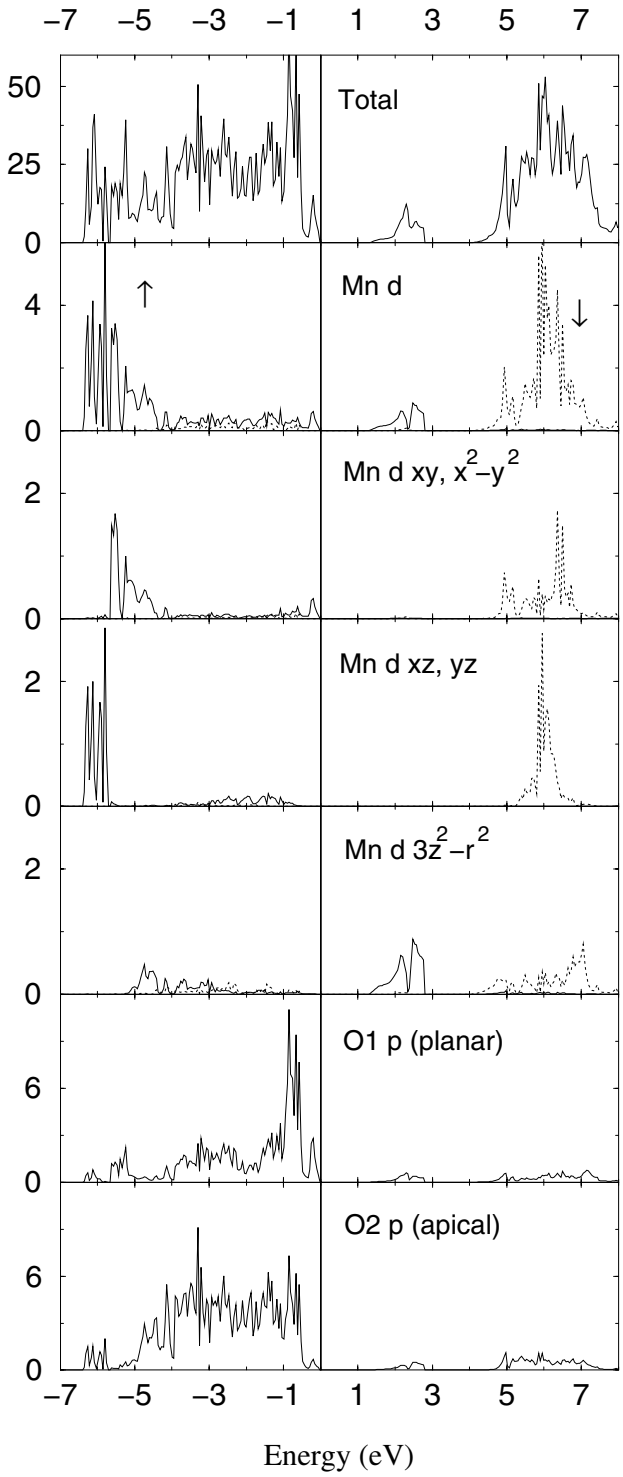


**Figure 3.** The total and partial densities of states (DOS) from the LSDA + $U$ calculation of the high-temperature AFM phase. Solid lines are for majority spin and dashed lines for minority spin.

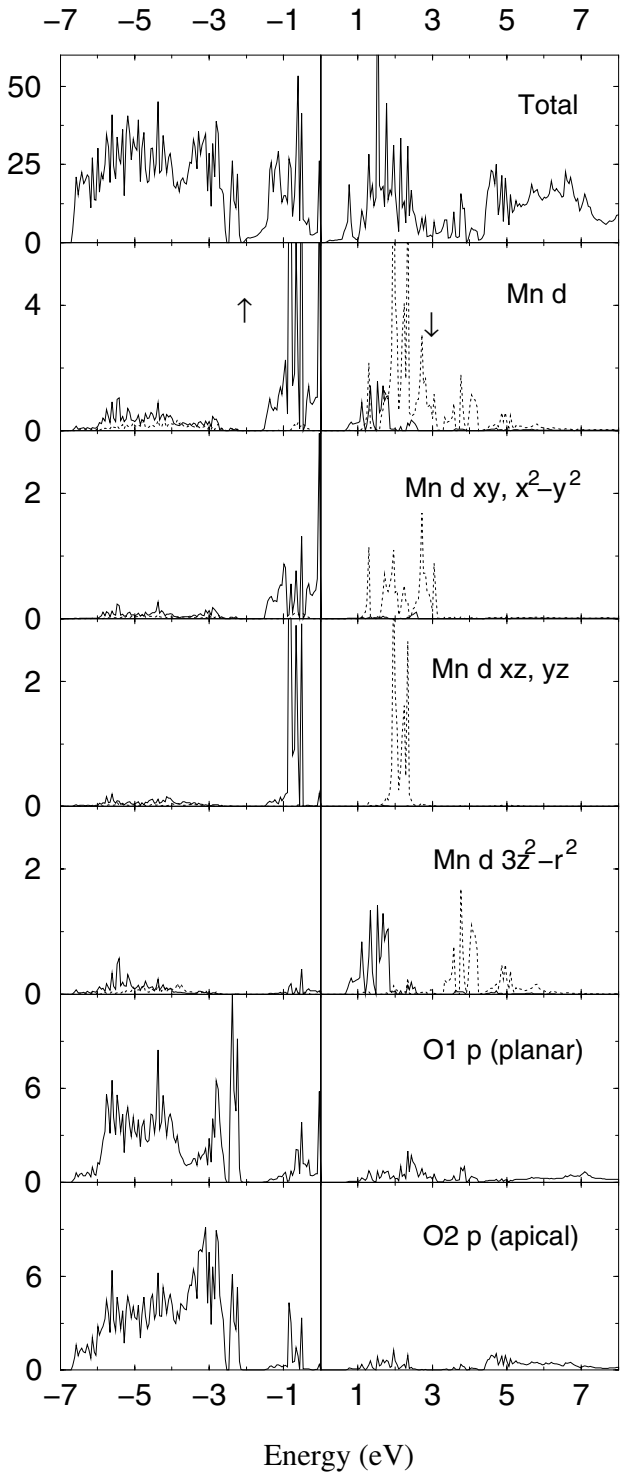


**Figure 4.** The total and partial densities of states (DOS) from the LSDA calculation of the low-temperature AFM phase. Solid lines are for majority spin and dashed lines for minority spin.

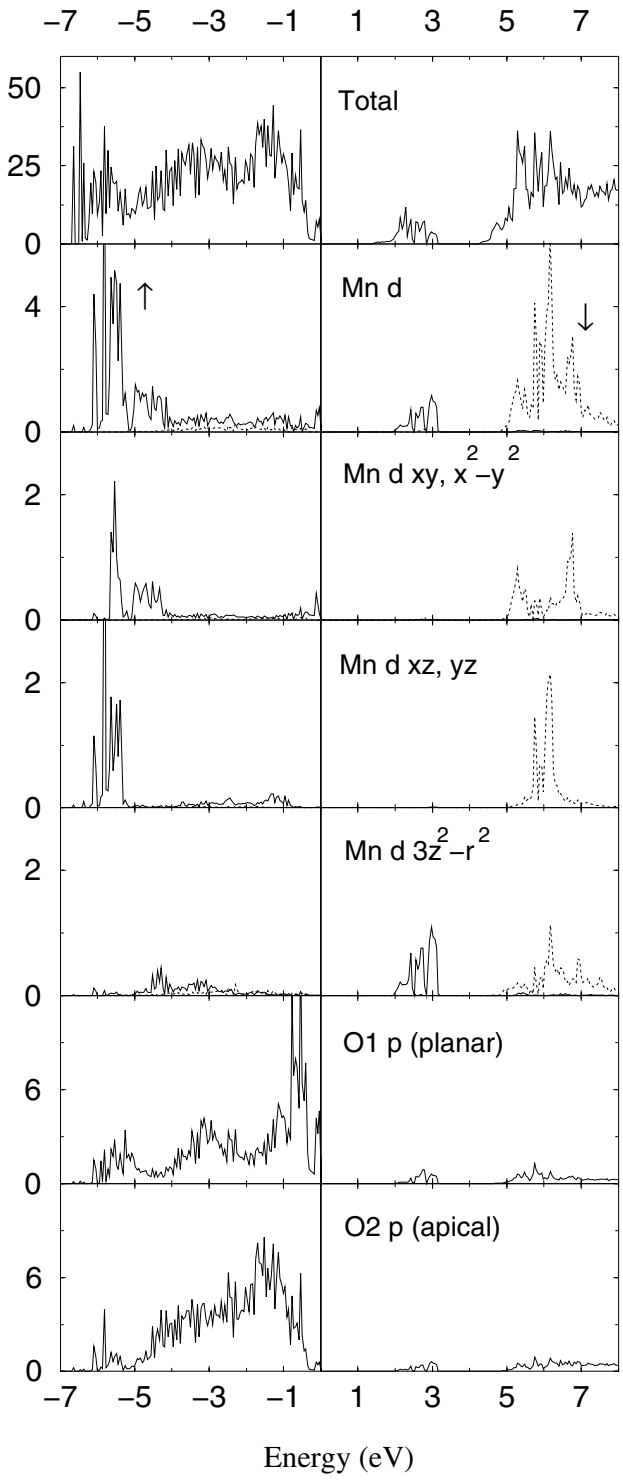


**Figure 5.** The total and partial densities of states (DOS) from the LSDA + $U$ calculation of the low-temperature AFM phase. Solid lines are for majority spin and dashed lines for minority spin.

is very similar to the ferroelectric mechanism in the perovskite ferroelectrics where the p–d hybridization and the long-range Coulomb interaction play an important role in driving the system from its high-symmetry configuration [24].

In order to illustrate the orbital polarization present in the high- and low-temperature phases, we have plotted the angular distribution of the majority-spin hole density:

$$\rho(\theta, \phi) = \sum_{mm'} (1 - n^{\uparrow}_{mm'}) Y_m(\theta, \phi) Y_{m'}(\theta, \phi) \tag{1}$$

where $n^{\uparrow}_{mm'}$ is the majority-spin occupation matrix. Since a $Mn^{3+}$ $d^4$ ion has formally two filled e levels and the empty $a_1$ state, the $a_1$ spin density must correspond to the density of this hole. The orbital ordering of Mn ions is presented graphically by plotting in figure 6(a), 6(b) the angular distribution of the majority-spin hole density according to equation (1). Figure 6(a) shows the orbital ordering of Mn ions (belonging to the $z$-plane) in the $MnO_5$ bipyramids of the high-temperature phase of $YMnO_3$. In the low-temperature phase, there is a tilting of the $MnO_5$ bipyramids with respect to the $c$-axis and a stronger distortion (figure 6(b)). Due to the shortest Mn–O bond with planar oxygen being along the $y$-axis, the corresponding $yz$-orbital is mixed with $3z^2 - r^2$ and the resulting majority-spin hole resides on an effective orbital, $\phi = 0.98(3z^2 - r^2) + 0.18yz$. We have found no orbital ordering in hexagonal $YMnO_3$.

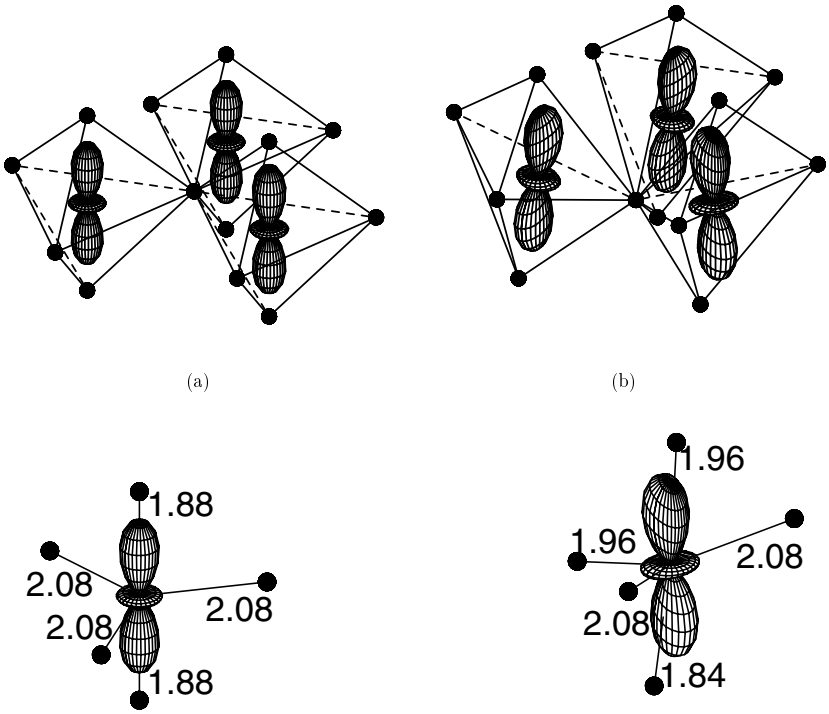


**Figure 6.** The calculated angle distortion of the $a_1$ hole spin density in high-temperature (a) and low-temperature (b) AFM phases of $YMnO_3$.

Finally, using the Green function method, we calculated the effective exchange interaction parameters in the LSDA + $U$ approach as a second derivative of the ground-state energy with respect to the magnetic moment rotation angle [25]. These parameters characterize the stability of the assumed magnetic configuration and so serve here as additional evidence for the reliability of these calculations. The value of the d–d effective exchange parameters for

nearest neighbours, $J_{dd}$, was found to be equal to 8 K. Then, we estimated the Néel temperature from the mean-field expression $T_N = J_{dd} z S(S+1)/3$, where $z$ is the coordination number of the magnetic ion in the lattice ($z = 6$ in our case) and $S = 2$. We obtained $T_N = 96$ K, which is in reasonable agreement with the experimental value, $T_N = 80$ K [6].

## 5. Conclusions

The electronic structure of hexagonal $YMnO_3$ in its high- and low-temperature phases was investigated by the LSDA and LSDA + $U$ methods. In striking contrast with the case for $LaMnO_3$, the Mn ion in hexagonal $YMnO_3$ is not in a JT electronic configuration. Due to the trigonal symmetry of the oxygen ions that are nearest neighbours of $Mn^{3+}$ ($d^4$), the highest d level, corresponding to the single hole in the spin-up d subshell, is non-degenerate as distinct from that of lanthanum manganite. We suggest that like that of $LaMnO_3$, the band pattern can be achieved in hexagonal $YMnO_3$ by divalent metal doping (hole doping).

A comparison of the results obtained for the FM and collinear AFM phases shows that an insulating ground state is predicted within the local density approximation for both crystal structures. This result allows one to conclude that magnetic ordering is critical to reproducing the band structure. The on-site Coulomb interaction separates the occupied and unoccupied Mn 3d bands and so has a significant influence on the band-gap formation and makes it comparable with experiment. This confirms that Coulomb correlations also make important contributions to the electronic structure—although we should emphasize here that the LSDA gives insulating states if proper magnetic ordering is taken into account. Further calculations, including ones for non-collinear triangular magnetic ordering, are desirable to separate the roles of magnetism and correlation effects. Nevertheless, the present calculations can be viewed as giving a good approximation to the correct non-collinear state, as follows from the band-structure results and estimates of the exchange interaction parameters.

## Acknowledgments

The work at Northwestern University was supported by the US Department of Energy (Grant No DF-F602-88ER45372) and by a grant of computing time at NERSC supercomputers. The work in Russia was supported by grants RFFI-98-02-17275 and 96-15-96598.

## References

[1] Bertaut E F, Forrat E F and Pang P 1963 *C. R. Acad. Sci., Paris* **256** 1958
[2] Yakel H L, Coehler W C, Bertaut E F and Forrat E F 1963 *Acta Crystallogr.* **16** 957
[3] Smolenskii G A and Chupis I E 1982 *Sov. Phys.–Usp.* **25** 475
[4] Ismailzade I G and Kizhaev S A 1965 *Sov. Phys.–Solid State* **7** 236
[5] Lukaszewicz K and Karut-Kalicinka J 1974 *Ferroelectrics* **7** 81
[6] Huang Z J, Cao Y, Sun Y Y, Xue Y Y and Chu C W 1997 *Phys. Rev.* B **56** 2623
[7] Wood V E, Austin A E, Collings E W and Brog K C 1973 *J. Phys. Chem. Solids* **35** 859
[8] Ismailzade I G, Smolenskii G A, Nesterenko V I and Agaev F A 1971 *Phys. Status Solidi* **5** 83
[9] Pickett W E and Singh D J 1996 *Phys. Rev.* B **53** 1146
[10] Solovyev I, Hamada N and Terakura K 1996 *Phys. Rev. Lett.* **76** 4825
[11] Fujimura N, Azuma S I, Aoki N, Yoshimura T and Ito T 1996 *J. Appl. Phys.* **80** 7084
[12] Fu B, Hubner W, Trubelja M F and Stubican V S 1994 *J. Mater. Res.* **9** 2645
[13] Satpathy S, Popović Z S and Vukajlović F R 1996 *Phys. Rev. Lett.* **76** 960
[14] Anisimov V I, Elfimov I S, Korotin M A and Terakura K 1997 *Phys. Rev.* B **55** 15 494
[15] Anisimov V I, Zaanen J and Andersen O K 1991 *Phys. Rev.* B **44** 943
Anisimov V I, Aryasetiawan F and Lichtenstein A I 1997 *J. Phys.: Condens. Matter* **9** 767

[16] Andersen O K 1975 *Phys. Rev.* B **12** 3060
[17] von Barth U, Hedin L and Janak B 1975 *Phys. Rev.* B **12** 1257
[18] Bertaut E and Mercier M 1963 *Phys. Lett.* **5** 27
[19] Sikora W and Syromyatnikov V N 1986 *J. Magn. Magn. Mater.* **60** 199
[20] Flurry R L 1983 *Quantum Chemistry* (Englewood Cliffs, NJ: Prentice-Hall) p 448
[21] Gunnarsson O, Andersen O K, Jepsen O and Zaanen J 1989 *Phys. Rev.* B **39** 1708
[22] Anisimov V I and Gunnarsson O 1991 *Phys. Rev.* B **43** 7570
[23] Kritayakirana K, Berger P and Jones R V 1969 *Opt. Commun.* **1** 95
[24] Inbar I and Cohen R E 1996 *Phys. Rev.* B **53** 1193
[25] Lichtenstein A I, Zaanen J and Anisimov V I 1995 *Phys. Rev.* B **52** R5467